Nickel-Molybdenum Hydrogen Evolution and Oxidation Reaction Electrocatalyst obtained by Electrospinning

Giovanni Ferro[1], Joseph Kalaus[2], Jiazhe Loki Chen[1], Eamonn Murphy[1], Lawrence Kulinsky[2] and Plamen Atanassov[1*]

[1]Department of Chemical and Biomolecular Engineering, University of California, Irvine, California 92697, USA

[2]Department of Mechanical and Aerospace Engineering, University of California, Irvine, California 92697, USA

Abstract

To accelerate the deployment of anion exchange membrane (AEM) technologies, and break free from our reliance on expensive and rare platinum group metals (PGM), this study explores a novel family of non-PGM electrocatalysts capable of both hydrogen evolution and oxidation. By thermal reduction, nanoparticles of nickel-molybdenum, 9:1 atomic ratio, were grown on fibrous carbon supports obtained by electrospinning and doped with carbon nanotubes (CNT). Complimentary characterization techniques confirm the integration of the CNT with the carbon fibers and a high loading of active alloy material on the support. In particular, XANES indicates a strong interaction between NiMo and the CNT. When supported on undoped carbon fibers, NiMo shows superior activity towards the hydrogen oxidation reaction (HOR) compared to the doped carbon supports. However, heat treating the catalysts in 10% NH_3/ 90% N_2 upsets this trend, while also improving the HOR performance of all the catalysts based on several performance indicators. In the case of NiMo on carbon fibers containing 7 wt% CNT, denoted as NiMo/CF(7%), the ammonia heat treatment produced a five-fold increase in the kinetic current. The catalysts NiMo/CF(7%)-NH_3 and NiMo/CF(24%)-NH_3, also capable of hydrogen evolution, match other state-of-the-art PGM-free HOR catalysts for their remarkable specific activity.

Keywords: Hydrogen oxidation, hydrogen evolution, alkaline media, nickel-molybdenum, alloy, carbon support, electrospinning, carbon nanotubes, nickel nitride, electrocatalysis

Introduction

Scientific advances in energy systems are driving the large-scale deployment of proton exchange membrane (PEM) fuel cells and electrolyzers, enabling realization of the vision of a carbon-free future.[1,2] Still, these devices suffer from reliance on scarce platinum group metals (PGM) to achieve industrially relevant reaction rates.[3] A promising alternative to PEMs are anion exchange membranes (AEMs), which operate in alkaline media and transport hydroxyl moieties.[4] While not efficient as PEMs, AEMs continue to gain interest due to their lower cost as compared to PEM technologies, requiring PGM catalysts.[5] Interestingly, in alkaline electrolyzers the activity of Pt for the hydrogen evolution reaction (HER) drops to a level comparable to PGM-free alternatives, making the search for these non-noble competitors particularly appealing.[2,4] Ultimately, the transition from acidic to alkaline environments opens the field of electrocatalysis to new challenges, the greatest of all being the discovery of a PGM-free catalyst capable of both hydrogen evolution and oxidation.[6]

Nickel has been shown to stand out amongst other transition metals for its inherent ability to catalyze the HER and the hydrogen oxidation reaction (HOR).[1,2,5,7–9] Its abundance and appreciable resistance to corrosion justify the increased attention that nickel and its alloys have received, especially for the HOR, the slower of the two reactions.[7] Still, to the best of our knowledge, a nickel-based catalyst able to outperform, or even match, state-of-the-art PGM materials has yet to be identified.[10] All the more worrisome is that the HOR remains orders of magnitude slower in alkaline than in acid, even with the most active Pt catalysts, presenting a substantial hurdle to AEM deployment.[11]

Here we report on a family of novel PGM-free HER/HOR catalysts obtained by growing nickel-molybdenum (NiMo) nanoparticles on electrospun carbon-based supports. Small amounts of multi-walled carbon nanotubes (CNT), namely 7, 13 and 24 wt%, were

suspended in the electrospinning solutions to give CNT-doped carbon fibers. Furthermore, we investigated the effect of a heat treatment in 10% NH_3 on the HER and HOR performance. Catalytic activities were measured in 0.1 M NaOH (semiconductor grade) at 20°C by a rotating disk electrode. All catalysts saw increased HOR activity after the heat treatment in NH_3, with a five-fold increase observed for ammonia treated NiMo on fibers containing 7 wt% CNT. CNT-doping of the carbon fiber supports also slightly improved the HOR performance. Catalysts with the highest HOR activities also showed superior HER capabilities. These catalysts outperformed most reported PGM-free HOR materials based on experimentally determined current densities.

Methodology

Materials

Polyacrylonitrile (PAN, average Mw 150,000), nickel(II) nitrate hexahydrate, ammonium heptamolybdate tetrahydrate, carbon nanotube multi-walled (CNT, >90% carbon basis, D x L 110-170 nm x 5-9 • m), platinum on graphitized carbon (Pt/C, 10 wt. % loading) and sodium hydroxide (NaOH, pellets, semiconductor grade, 99.99% trace metal basis) were purchased from Sigma Aldrich. N,N-dimethylformamide (DMF) was purchased from Fisher Chemical and Ketjenblack EC-600JD (KB, 1400 m^2/g) was purchased from Nouryon (formely AkzoNobel). Isopropyl alcohol (IPA, ACS grade) and Sustainion® XC-1 ionomer solution (5% in ethanol) were obtained from Macron Fine Chemicals and Dioxide Materials, respectively. All chemicals were used as received without further purification. Deionized water (DI) in our lab has a resistivity of 18.2 M• cm at 25 ºC and a total organic content that does not exceed 5 ppb.

Synthesis of the carbon fiber support

In a typical synthesis, 1.3 g of PAN were added to 18.7 g of DMF (6.5 wt% PAN) and stirred vigorously for at least 18 hours in a sealed glass vial at 70ºC. The clear solution was electrospun using a setup consisting of a computer controlled grounded roller covered in aluminum foil (All Motion), a syringe pump (Harvard Apparatus), a syringe (BD), and a computer controlled high power voltage supply (WaveForms) (Fig. 1g and Fig. S1). The temperature during electrospinning was kept at 25ºC and the relative

humidity at 40%. A 10 ml syringe with an inner diameter of 14.55 mm and a tip of 20 gauge (Jensen Global) was loaded with the PAN solution. The loaded syringe was positioned at a horizontal distance of 15 cm from the roller to the syringe tip. The vertical distance from the floor of the case to the syringe tip was 17 cm. An electric field was applied by connecting the high-voltage power supply to the syringe tip, with a voltage of around 15 kV. The polymer solution was pumped through the syringe at a constant flow rate of 0.010 ml/min using a syringe pump. Simultaneously, the roller was rotated at a speed of 400 rpm to collect the fibers evenly. The fibers were removed from the aluminum foil and stabilized in air at 300ºC for one hour, followed by natural cooling. The heating to 300ºC was achieved in two steps: from 20ºC to 230ºC with a ramp rate (rr) of 70ºC hr^{-1} and from 230ºC to 300ºC with a ramp rate of 23.3ºC hr^{-1}. The stabilized fibers were treated at 600ºC (rr 4.8ºC min^{-1}) for one hour in ultra high purity nitrogen (Airgas) before they were naturally cooled. The fibers, now dark gray and brittle, were ground by pestle and mortar and heat treated in 5% hydrogen, balance argon (Airgas) at 975ºC for 45 min, followed by natural cooling. The heating to 975ºC was achieved in three steps: from 20ºC to 525ºC (rr 105ºC min^{-1}), from 525ºC to 900ºC (rr 31.3ºC min^{-1}) and from 900ºC to 975ºC (rr 9.4ºC min^{-1}). The obtained carbon fiber support was labeled CF(0%).

Synthesis of the CNT-doped carbon fiber supports

The synthesis is identical to the previous procedure except that various amounts of CNT were added to the PAN-DMF solution once the polymer had completely dissolved. Three types of CNT-doped carbon fibers were prepared with nominal CNT loadings of 7, 13 and 24 wt%. These carbon supports are denoted CF(7%), CF(13%) and CF(24%). The amount of PAN in each solution was kept at 6.5 wt% by decreasing the mass of DMF in accordance with the mass of CNT being added. For example, for fibers containing 24 wt% CNT, the electrospinning solution consisted of 1.3 g of PAN, 18.3 g of DMF and 0.4 g of CNT.

Synthesis of NiMo/KB

In a typical synthesis, 2.096 g of nickel(II) nitrate hexahydrate and 0.141 g of ammonium heptamolybdate tetrahydrate (Ni:Mo atomic ratio 9:1) were dissolved in 40 ml of DI under gentle stirring followed by the addition of 0.5 g of KB. The solution was bath sonicated on high power for 20 min, stirred vigorously for 20 min and then dried in air at 70ºC for at least 24 hours. The mixture was ground by pestle and mortar and thermally reduced in 5% hydrogen, balance argon (Airgas) at 550ºC (rr 5ºC min^{-1}) for one hour before it was naturally cooled. Finely divided Ni is pyrophoric, hence special attention was paid during the removal of the catalyst from the tube furnace and first exposure to ambient atmosphere. Pyrophoricity was never observed during our syntheses. The obtained catalyst was labeled NiMo/KB.

Synthesis of NiMo/CF(X%), NiMo/CNT and Ni/KB

For NiMo/CF(X%) the synthesis is identical to the previous procedure except that carbon fiber supports CF(0%), CF(7%), CF(13%) and CF(24%) were used instead of KB. Four catalysts labeled NiMo/CF(X%) were obtained, where X = {0, 7, 13, 24} denotes the nominal wt% of CNT in the carbon fiber support. NiMo/CNT was synthesized identically to NiMo/KB but with CNT as the sole carbon support. Ni/KB was synthesized identically to NiMo/KB but in the absence of molybdenum.

NH_3 heat treatment

The catalysts NiMo/KB-NH_3, NiMo/CF(X%)-NH_3 and NiMo/CNT-NH_3 were obtained by heat treating the precursor catalysts (ie. without "-NH_3") in 10% ammonia, balance nitrogen (Airgas), with a flow rate of 150 mL min^{-1}. The catalysts were kept at 350ºC for three hours (rr 10ºC min^{-1}) and then naturally cooled.

Physical Characterization

The morphology and nano structure of CF(7%) was analyzed by transmission electron microscopy (TEM) using a JEOL 2100F at an accelerating voltage of 200 kV. TEM was performed on the catalysts using a JEOL 2800 with an accelerating voltage of 200 kV. Furthermore, the atomic distribution of NiMo/KB was analyzed by aberration-corrected scanning transmission electron microscopy (AC-STEM) and energy dispersive X-ray

spectroscopy (EDS) using a JEOL ARM300CF at an accelerating voltage of 300 kV. X-ray diffraction (XRD) data were collected using a Rigaku Ultima III Powder X-ray diffractometer with a 1.2 kW Cu Kα source (λ = 0.15405 nm). X-ray Absorption Near Edge Structure (XANES) data were collected using an easyXAFS300+ with a 1.2 kW liquid-cooled X-ray Tube as source and a Si 551 crystal analyzer. A Ni foil standard (6 microns thick) was used to correct the energy shift of all the structures.

Electrochemical Characterization

Electrochemical experiments were performed in a glass cell made by Adams & Chittenden in 0.1 M semiconductor grade NaOH electrolyte. The working electrode (WE) was a Pine Research PTFE separated and lined glassy carbon disc (0.247 cm^2). The counter electrode (CE), a carbon rod, was separated from the WE compartment by a glass frit. A hydrogen electrode (HydroFlex) from Gaskatel was used as reference. Tests were performed using a Pine Research rotator and a Bio-Logic VSP-300 potentiostat. All electrode potentials are reported versus the reversible hydrogen electrode (RHE).

The electrocatalytic activity of the catalysts was measured using a thin film approach. For HOR experiments catalyst inks was prepared by dispersing 4.88 mg of catalyst in 389 • L of DI, 100 • L of IPA and 4.5 • L of Sustainion solution. The suspension was sonicated at an amplitude of 30% two times for 15 s using a horn and then bath sonicated for at least 10 min. 12.5 • L of catalyst ink were drop-cast on a polished glassy carbon WE and dried in air at 70ºC for 15 min, followed by naturally cooling. The WE was conditioned by cyclic voltammetry in the potential range from –0.20 V to 0.40 V, for a total of 20 cycles, at a scan rate (•) of 20 mV s^{-1} in N_2 saturated electrolyte (Fig. S2). Three cyclic voltammograms (CV) were recorded between –0.06 V and 0.40 V with • = 20 mV s^{-1}. Another three CVs were recorded between –0.06 V and 0.40 V with • = 5 mV s^{-1} and a rotating speed of 1600 rpm; these three CVs were repeated in H_2 saturated electrolyte. Linear sweep voltammograms (LSV) in H_2 saturated electrolyte were obtained by scanning anodically from –0.06 V to 0.11 V with • = 5 mV s^{-1}; these were measured at rotation speeds of 400, 650, 900, 1600 and 2500 rpm. For HER experiments catalyst inks was prepared by dispersing 2.44 mg of catalyst in 979 • L of

DI, 252 • L of IPA and 2 • L of Sustainion solution. The thin film WE was prepared in the same way as for the HOR. The WE was conditioned by cyclic voltammetry in the potential range from –0.20 V to 0.40 V, for a total of 10 cycles, with • = 20 mV s^{-1} in N_2 saturated electrolyte. LSVs were obtained by scanning cathodically from 0.05 V to -0.6 V with • = 10 mV s^{-1} and a rotation speed of 2500 rpm. All potentials were corrected for uncompensated resistance using electrochemical impedance spectroscopy (EIS).

For a more accurate estimation the electrochemically active surface area (ECSA), cyclic voltammetry had to be performed on the bare carbon supports. 3 mg of carbon support were suspended in 971 • L of IPA and bath sonicated for 5 min. 10 • L of mixture were drop-cast on a polished glassy carbon WE, dried in air, and followed by another 10 • L drop-cast and air drying. The WE was cycled three times in the potential range from –0.20 V to 0.40 V with • = 20 mV s^{-1} in N_2 saturated electrolyte. Another three CVs were recorded between –0.06 V and 0.40 V. The ECSA was calculated from the CVs measured in N_2 saturated electrolyte in the window –0.06 V and 0.40 V with • = 20 mV s^{-1} and no rotation. Following the subtraction of the carbon support curve from the catalyst curve, the entire anodic charge was divided by 0.514 mC cm^{-2} to give an estimate of the ECSA for each catalyst (Fig. S3).

Exchange currents were calculated from the LSVs measured at 1600 rpm. The micro-polarization region (from -0.01 V to 0.01 V) was linearized (Fig. S4a) and the slope, m, used to calculate the exchange current, i_{xc}, as per the equation below.

$$i_{xc} = \frac{RT}{nF} m$$

where m has units A V^{-1}, n = 1, R = 8.3145 J mol^{-1} K^{-1}, T = 293.15 K and F = 96485 A s mol^{-1}. Recognizing that 1 J = 1 kg m^2 s^{-2} and that 1 V = 1 kg m^2 s^{-3} A^{-1}, we obtain i_{xc} in amperes. Exchange currents were normalized by metal mass and ECSA to capture mass activities, i_0, and specific activities, j_0, respectively. Kinetic currents at 0.1 V were calculated by Koutecký–Levich analysis (Fig. S4b).

Results and discussion

Catalyst Preparation

Eleven novel carbon-based supported electrocatalysts, comprised of NiMo with a 9:1 atomic ratio, were synthesized by a thermal reduction method. Briefly, fibrous carbon supports were obtained by electrospinning solutions of polyacrylonitrile (PAN) in dimethylformamide (DMF) containing varying amounts of CNT. After heat treatment, the carbonized fibers were combined with Ni and Mo precursors, with a target metal loading of 50 wt%, and thermally reduced in 5% H_2. The catalysts were labelled NiMo/CF(X%), where X denotes the wt% of CNT in the carbon fiber support. For example, NiMo/CF(7%) consists of NiMo nanoparticles supported on carbon fibers containing 7 wt% CNT, nominally. Ni and NiMo nanoparticles supported on Ketjenblack EC-600JD (KB) were also prepared and used as benchmarks.[1] All catalysts, with the exception of Ni/KB, were also synthesized with an additional heat treatment in 10% NH_3; these catalysts are given the suffix '-NH_3'. Table 1 summarizes the composition of the electrocatalysts synthesized and analyzed in this work.

Table 1. Summary of carbon supported nickel-based catalyst synthesized for this study.

Name	Description
Ni/KB	Ni nanoparticles (NP) on Ketjenblack EC-600JD (KB)
NiMo/KB	Ni-Mo NP (9:1 at.) on KB
NiMo/CF(0%)	Ni-Mo NP (9:1 at.) on carbon fibers (CF)
NiMo/CF(7%)	Ni-Mo NP (9:1 at.) on 7 wt% CF
NiMo/CF(13%)	Ni-Mo NP (9:1 at.) on 13 wt% CF
NiMo/CF(24%)	Ni-Mo NP (9:1 at.) on 24 wt% CF
NiMo/CNT	Ni-Mo NP (9:1 at.) on carbon nanotubes (CNT)

Suffix	Description
no suffix	Catalyst thermally treated in 5% H_2 / 95% Ar
-NH_3	Catalyst thermally treated in 5% H_2 / 95% Ar followed by a thermal treatment in 10% NH_3 / 90% N_2

Physical Characterization

Transmission electron microscopy (TEM) and X-ray diffraction (XRD) analysis confirm the successful incorporation of the CNT into the electrospun fibers (Fig. 1). Fig. 1a shows CNT decorated carbon fibers and the XRD in Fig. 1b positively correlates the graphitic content of the catalysts with the amount of CNT in the carbon support. TEM also reveals an appreciably homogeneous distribution of nanoparticles on the carbon support surface, despite the high nominal metal loading of 50 wt% (Fig. 2). In particular, the high surface area of KB enabled an excellent dispersion of the active material, with only a few clusters, maintaining an average particle size of 13 ± 2 nm (Fig. 2a). The widespread presence of metallic particles on the fibrous carbon supports was also confirmed, with slight agglomeration being observed (Fig. 2b and 2c).

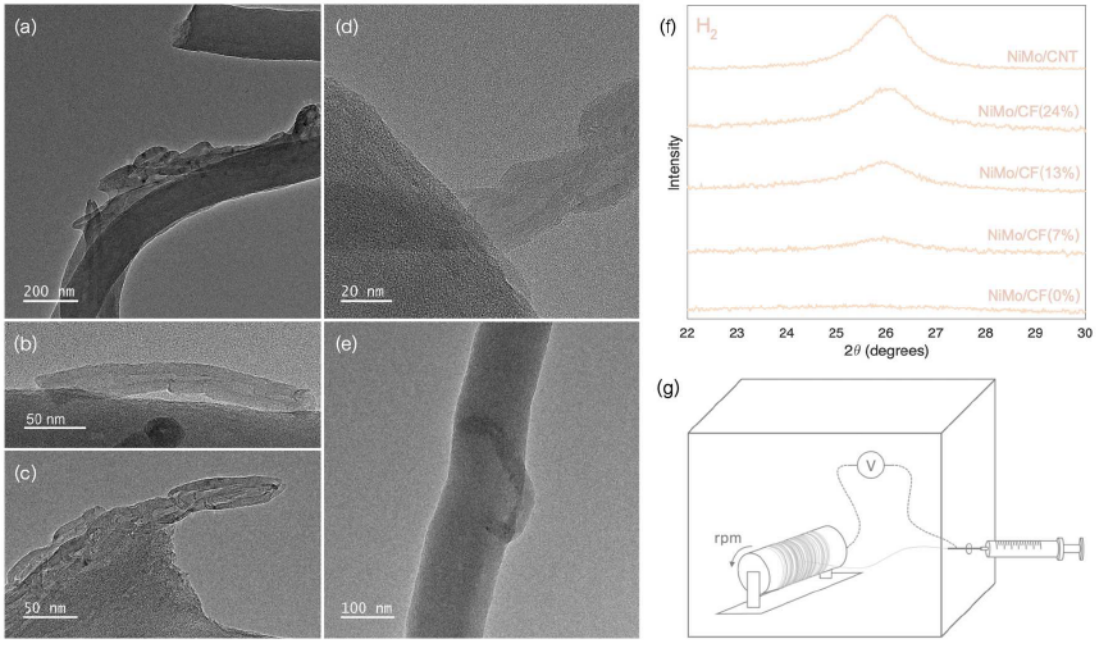

Figure 1. (a• e) TEM images of carbon fibers doped with CNT (7 wt%, nominally) before the addition of NiMo nanoparticles. The nanoparticles present within the CNT, most noticeable in the top-left and bottom-left images, are nickel impurities in the purchased CNT (Fig. S5). (f) X-ray diffraction patterns of the catalysts synthesized by thermal reduction in 5% H_2; zoom-in of the graphitic peak (2• of 26 degrees) shows the successful incorporation of highly graphitic CNTs into the fibrous carbon support. (g) Schematic of the electrospinning setup.

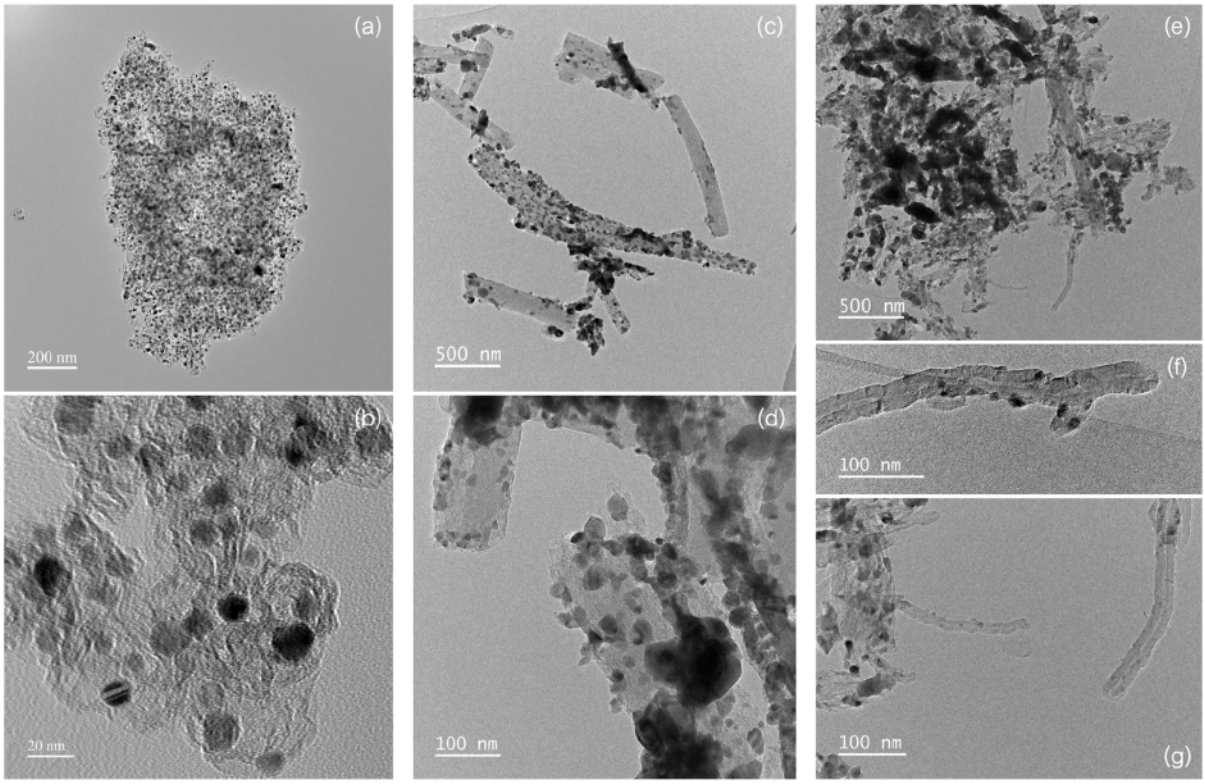

Figure 2. TEM images of (a,b) NiMo/KB, (c,d) NiMo/CF(0%) and (e• g) NiMo/CF(7%).

Confirmation of the NiMo alloy (9:1 atomic ratio) was established by energy dispersive X-ray spectroscopy (EDS), XRD and X-ray Absorption Near Edge Structure (XANES). The high angle annular dark field scanning transmission electron microscopy (HAADF-STEM) image of NiMo/KB, shown in Fig. 3a with its corresponding elemental mapping, confirms the presence of NiMo alloy nanoparticles supported on the carbon. The EDS spectrum in Fig. 3b displays a significantly higher EDS count for nickel compared to molybdenum, as expected for a 9:1 (Ni:Mo) atomic ratio. An EDS line scan over a nanoparticle generated a bell curve distribution of Ni counts and a constant distribution of Mo counts (Fig. 3c), implying the possibility of a surface enrichment in Mo. In 2017 Kabir et al. postulated on the Mo rich surface for NiMo alloyed nanoparticles based on XPS analysis.[1]

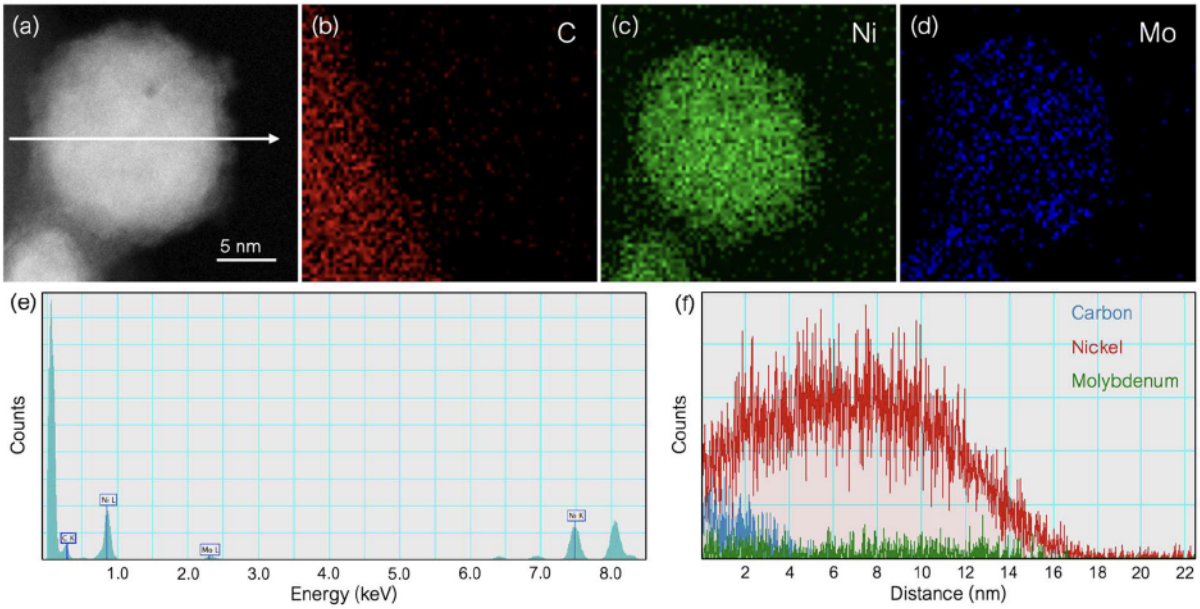

Figure 3. Elemental composition of a NiMo/KB nanoparticle. (a) HAADF-STEM image of a nanoparticle in NiMo/KB, (c• d) the corresponding EDS mapping and (e) spectrum. (f) EDS spectrum for the line scan performed along the white arrow shown in (a) over a NiMo nanoparticle.

The XRD pattern for molybdenum-free Ni/KB (Fig. 4a) establishes the presence of NiO in the bulk, in addition to Ni metal. In contrast, all NiMo catalysts, irrespective of their carbon support, show no or minimal bulk NiO, attributed to the ability of the highly oxyphilic Mo to protect Ni from oxidation. Additionally, the presence of metallic Mo results in a slight leftward shift of the Ni peaks. Calculated from XRD, the cubic nickel phase in Ni/KB has a lattice constant of 3.525 Å, in agreement with the literature.[12] Meanwhile, the calculated lattice constants for the NiMo catalysts in Fig. 4a lie between 3.533 Å and 3.541 Å, affirming that the presence of Mo marginally increases the lattice constant. The XRD patterns of catalysts heat treated in NH_3 are displayed in Fig. 4b. While all spectra are still dominated by the NiMo peaks at 2θ values of 44.3, 51.5 and 76, nickel nitride signals emerge for some catalysts as a result of the NH_3 heat treatment. Specifically, bulk Ni_4N is increasingly present in NiMo/CF(7%), NiMo/CF(24%) and NiMo/CF(0%), with the latter also containing some Ni_3N.

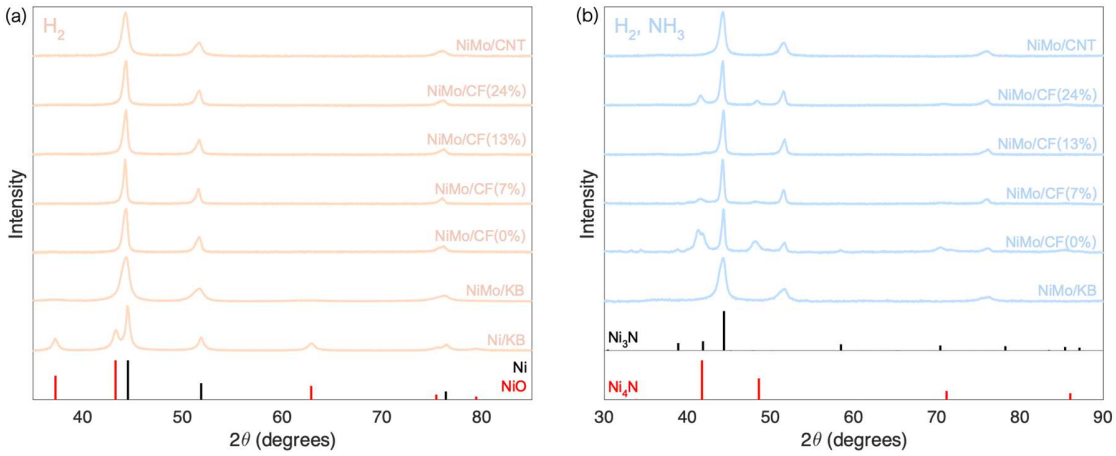

Figure 4. X-ray diffraction patterns of catalysts synthesized by (a) thermal reduction in 5% H_2, balance Ar and (b) thermal reduction in 5% H_2, balance Ar, followed by a heat treatment in 10% NH_3, balance N_2.

XANES analysis of the Ni K edge (8333 eV) for select catalysts are shown in Fig. 5. The presence of bulk NiO (Ni^{2+})nin Ni/KB is confirmed in Fig. 5a, showing the Ni/KB K edge shifting to a higher energy relative to the Ni foil (Ni^0) and peaking sharply around 8350 eV.[13] Conversely, NiMo/KB shows a smaller energy shift than Ni/KB relative to the Ni foil and a lower peak at 8350 eV. This can be attributed to the ability of highly oxyphilic Mo to protect Ni from oxidation, corroborated by XRD. Most evident from the XANES plot in Fig. 5a is the shift to lower energies for CNT containing catalysts. In fact, NiMo/CF(7%), NiMo/CF(24%) and NiMo/CNT all exhibit edges significantly lower energies compared to the Ni foil. Although full understanding of this phenomenon would require further characterization, we hypothesize these observed shifts result from the presence of highly graphitic CNTs, whose sp^2-hybridized carbons behave as electron donors and create a reductive environment for the Ni. These large energy shifts are consistent with the successful incorporation of CNTs into the carbon support (and consequently into the catalyst matrix), and with electronic interactions between CNT and NiMo nanoparticles.

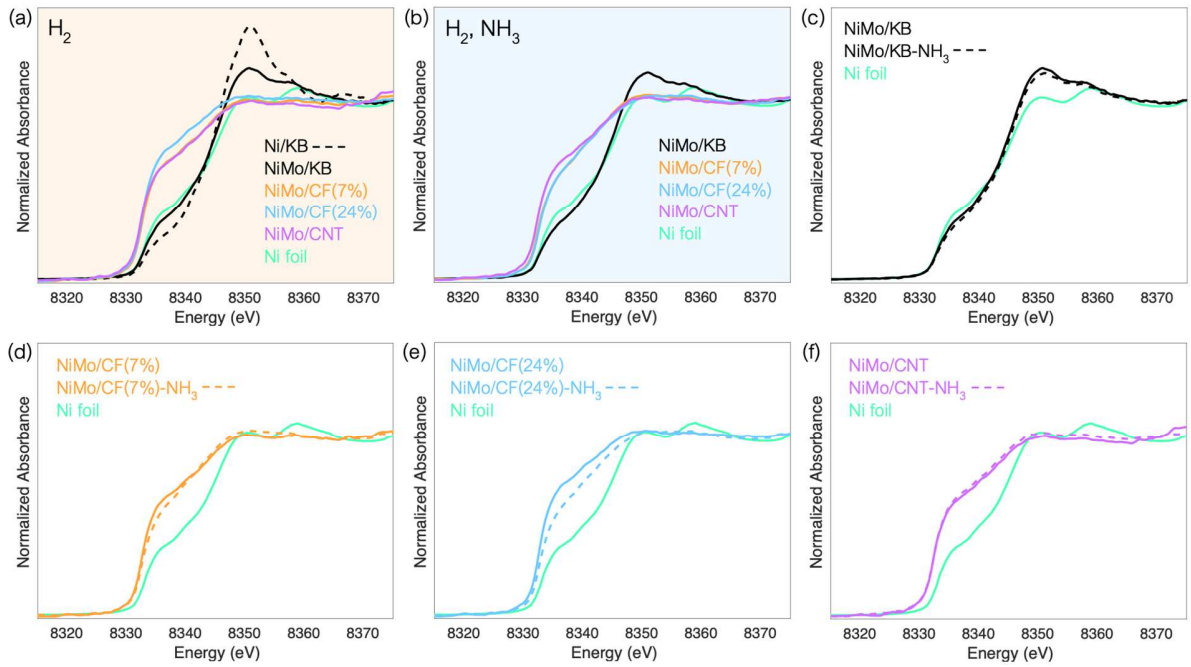

Figure 5. XANES of the Ni K edge at 8333 eV for select catalysts synthesized by (a) thermal reduction in 5% H_2, balance Ar and (b) thermal reduction in 5% H_2, balance Ar, followed by a heat treatment in 10% NH_3, balance N_2. Direct comparison of the Ni K edge with and without heat treatment in ammonia for (c) NiMo/KB, (d) NiMo/CF(7%), (e) NiMo/CF(24%) and (f) NiMo/CNT.

XANES was also used to investigate the effect of the heat treatment in NH_3 on the electronic structure of the catalysts. From Fig. 5b, direct comparison of near edge structures before and after the treatment reveals that catalysts containing nickel nitride saw small shifts to higher energies (Fig. 5c-f). In particular, NiMo/CF(7%)-NH_3 and NiMo/CF(24%)-NH_3 both saw a shift to higher energy, relative to the Ni foil, in accordance with the oxidative effect of nitrogen, a highly electronegative element. The change was larger for NiMo/CF(24%)-NH_3, in agreement with the XRD that this catalyst contained a larger amount of Ni_4N relative to NiMo/CF(7%)-NH_3 (Fig. 5c-d). The observed XANES shift associated with the formation of nickel nitride supports the works of Ni et al. and Song et al., both reporting positive Ni $2p_{3/2}$ binding energy shifts for Ni_3N in XPS.[2,8] Specifically, Song et al. measured a shift from 852.4 eV to 853.3 eV as a result of surface Ni_3N formation, which they believe to contain Ni(I) species.[2] Similarly, Ni et al. report a binding energy of 853 eV for Ni_3N, which they ascribe to the presence

of partially positive Ni(+δ), akin to the nickel found in Ni_2P.[8] Despite XANES and XPS being different spectroscopic techniques, their data in this case coalesce when probing very similar electronic structures. Furthermore, based on our XRD and XANES analysis, capable only of bulk characterization, the presence of nickel nitride on the surface of NH_3 treated catalysts cannot be confirmed nor excluded.

Electrochemically Active Surface Area

The electrochemically active surface area (ECSA) of each catalyst was estimated experimentally by cyclic voltammetry (Fig. 6). Of the catalysts pyrolyzed only in H_2 (Fig. 6, orange), Ni/KB shows the smallest ECSA likely due to increased sintering during the thermal reduction, given that no thermal energy could go towards alloy formation. Conversely, NiMo/KB displays the largest ECSA, namely 8.4 ± 1.0 cm^2, attributed to the excellent dispersion of the nanoparticles on the carbon support, as observed in TEM. The decreased ECSA for NiMo/CF(0%) and NiMo/CF(7%) agrees with the reduced metal dispersion (more agglomeration) observed in TEM for these catalysts; a similar effect can be hypothesized for NiMo/CF(13%) and NiMo/CF(24%). In particular, we postulate that the small diameter of the CNT presents a challenge for the formation of NiMo nanoparticles on these tubes and forces more nanoparticles to deposit on the carbon fibers. This is in agreement with TEM micrographs showing fewer and smaller nanoparticles on the CNTs, meanwhile agglomeration develops on the fibers. The slightly increased ECSA for NiMo/CNT is likely due to the formation of CNT agglomerates or 'islands' favoring the formation of NiMo nanoparticles. Furthermore, since the CNT are smaller in diameter than the carbon fibers (ca. 50 nm and >100 nm, respectively, by TEM) this results in a much higher surface area per unit mass, counteracting area loss due to agglomeration, and resulting in still an appreciably large surface area for the dispersion of the nanoparticles.

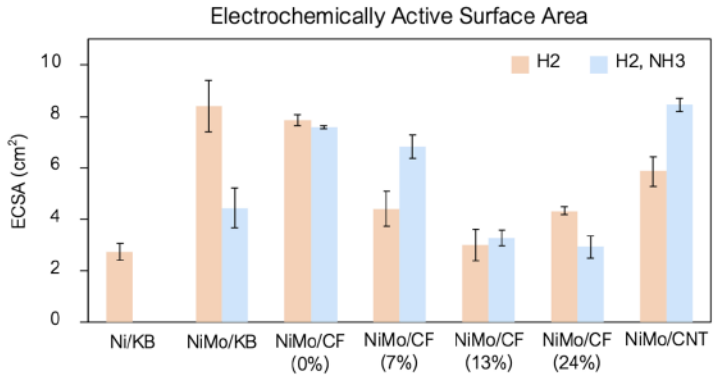

Figure 6. ECSA estimated by CVs obtained in N_2 saturated 0.1M NaOH between –0.06 V and 0.40 V at a scan rate of 20 mV s^{-1}. The charge associated with the formation of a monolayer of α-$Ni(OH)_2$ was calculated by subtracting the charge related to the carbon support from the total anodic charge. This difference was divided by 0.514 mC cm^{-2} to give an estimate of the ECSA for each catalyst. The catalyst loading is 500 • g cm^{-2}. Error bars represent standard deviations of three independent experiments.

After the NH_3 heat treatment (Fig. 6, blue), during which the catalyst was held at 350°C for 3 hours, NiMo/KB-NH_3 saw a 47% decrease in ECSA, which is largely attributed to sintering. It is likely that the small particles of NiMo/KB are highly susceptible to agglomeration. The formation of surface Ni_3N could also be responsible for the decreased ECSA, however this could not be confirmed spectroscopically. The other catalysts show similar ECSA before and after NH_3 heat treatment, with the exception of NiMo/CF(7%) and NiMo/CNT. It is possible the ECSA is overestimated for these catalysts due to their superior HER and HOR performance interfering with the electrochemical determination of the ECSA (Fig. S6).

HOR Performance

The HOR performance of all thirteen catalysts was evaluated using a rotating disk electrode (RDE), from which three distinct performance quantifiers were obtained: (1) the current density achieved at 0.1 V and a rotation speed of 1600 rpm, (2) the exchange current density at 1600 rpm and (3) the kinetic current density at 0.1 V. The exchange and kinetic current densities were normalized by the metal mass and ECSA

to capture mass and specific activities, respectively. CVs measured in N_2 and H_2 saturated electrolyte (Fig. S7) reveal that all catalysts show some activity towards the HOR. Catalysts pyrolyzed only in H_2 (Fig. 5a) produced CVs typical for Ni-based catalysts, featuring decaying currents past 0.12 V and the inability to reach diffusion limiting currents observed for Pt-based electrodes.[14,15] This undesirable, yet typical behavior is also observed for some precious metal catalysts such as Ru/C and has been associated with the formation of surface □-$Ni(OH)_2$, which promptly follows the oxidation of Ni to non-stoichiometric NiO_x occurring around 0.2 V.[16][4][17][18] The soft peak around 0.24 V seen for most CVs in Fig. 7 can therefore be attributed to the formation of a monolayer of □-$Ni(OH)_2$, which, is known to be reversible and was confirmed in this work (Fig. S8).[1] The molybdenum free Ni/KB is not protected from oxidation, hence the current decay beginning before 0.1 V. Moreover, in N_2 saturated electrolyte, where Ni chemistry is evidenced over hydrogen's, the oxidation of Ni occurs tens of millivolts before the oxidation of NiMo (Fig. S9). This delay in the passivation of Ni is desirable, as it enables the catalyst to operate at higher anodic potentials where higher currents can be achieved.[8] Catalysts heat treated in NH_3 achieved higher currents (Fig. 5b), with NiMo/CF(7%)-NH_3 seeing a three-fold increase in the current density at 0.1 V (Fig. 8). Still, even for these catalysts, diffusion limiting current densities were not achieved and current decay was observed at more oxidative potentials.[19] Fig. 8 summarizes the current densities achieved at 0.1 V in H_2 saturated 0.1 M NaOH with a rotating speed of 1600 rpm and a scan rate of 5 mV s^{-1}. At 0.1 V NiMo/CF(7%)-NH_3 and NiMo/CNT-NH_3 share the same maximum current density of 1.51 ± 0.04 mA cm^{-2}, surpassing Pd/C and Ru/C (1.25 and 1.4 mA cm^{-2}) as well as NiMo on 2D-MXene (1.47 mA cm^{-2}), under equivalent conditions.[6,15,16]

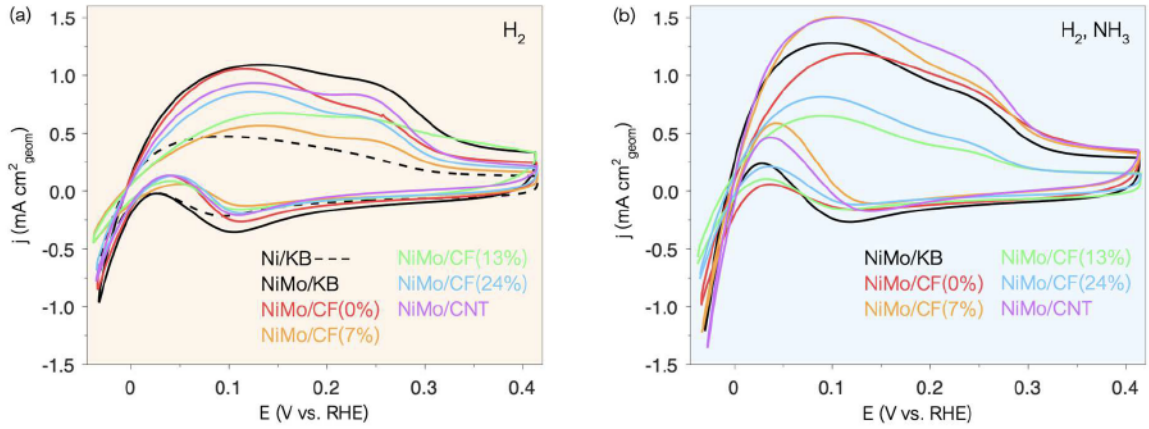

Figure 7. CVs measured between –0.06 V and 0.40 V in H_2 saturated 0.1M NaOH at a scan rate of 5 mV s^{-1}, a rotating speed of 1600 rpm and a catalyst loading of 500 • g cm^{-2}. Catalysts synthesized by (a) thermal reduction in 5% H_2, balance Ar and (b) thermal reduction in 5% H_2, balance Ar, followed by a heat treatment in 10% NH_3, balance N_2. Thermally treating the catalysts in NH_3 increases the HOR activity. Curves are averages of three independent experiments.

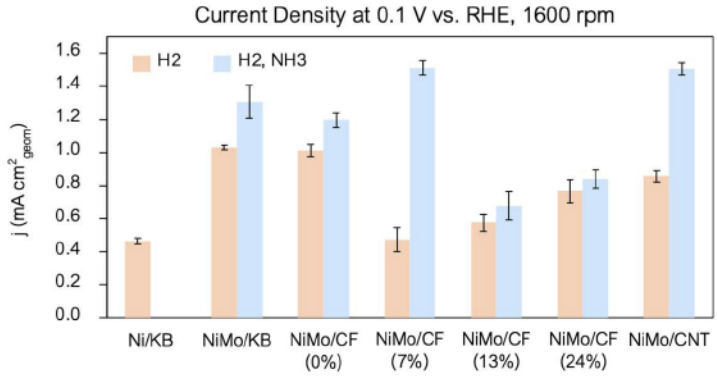

Figure 8. Current densities normalized by the electrode surface area, achieved at 0.1 V during the anodic sweep of CVs obtained between –0.06 V and 0.40 V, with a scan rate of 5 mV s^{-1}, in H_2 saturated 0.1M NaOH. The rotating speed was 1600 rpm and the catalyst loading was 500 • g cm^{-2}. Error bars represent standard deviations of three independent experiments.

LSVs measured at different rotating speeds confirm the high HOR activity of the catalysts (Fig. S10). The rotating speed dependence on the anodic currents for NiMo/KB (Fig. 9a) is strengthened by the NH_3 heat treatment (Fig. 9b) indicating an improvement in the HOR performance. This kind of enhancement is observed for all catalysts (Fig. S10) and is most evident for NiMo/CF(7%) as shown in Fig. 9c-d. Interestingly, Ni/KB (Fig. S10) shows a minimal current dependence on the rotation speed given that slight anodic potentials rapidly quench its catalytic ability, owed to the formation of surface α-$Ni(OH)_2$.

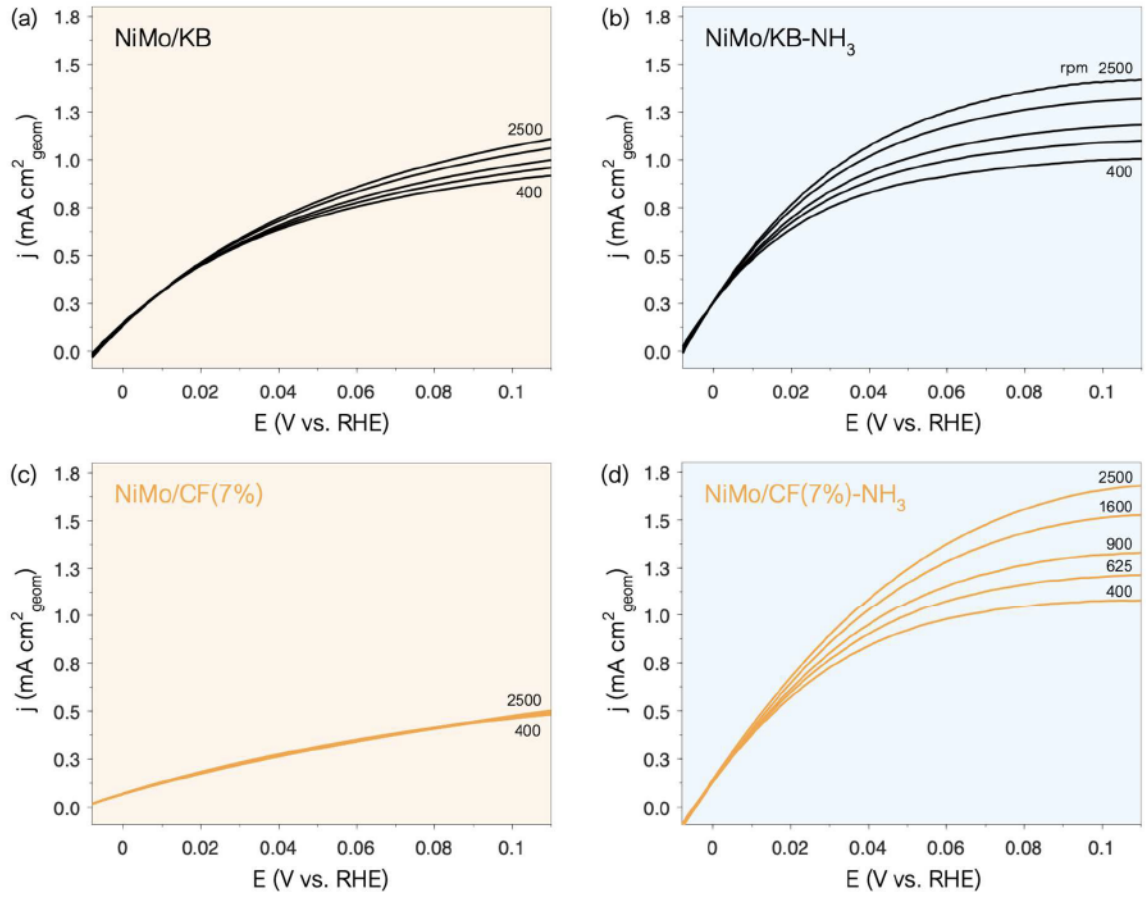

Figure 9. LSVs measured between –0.06 V and 0.11 V in H_2 saturated 0.1M NaOH at a scan rate of 5 mV s^{-1}, a catalyst loading of 500 • g cm^{-2}, and various rotating speeds (400, 625, 900, 1600 and 2500 rpm). (a) and (c) belong to catalysts NiMo/KB and NiMo/CF(7%), respectively, subjected only to a thermal reduction in 5% H_2, balance Ar. (b) and (d) belong to catalysts NiMo/KB and NiMo/CF(7%), respectively, that were also thermally treated in 10% NH_3, balance N_2. Thermally treating the catalysts in NH_3

increases the HOR activity; in the case of NiMo/CF(7%) this increase is substantial. Curves are averages of three independent experiments.

Mass weighted exchange current densities were calculated for each catalyst using a nominal metal loading of 250 • g cm^{-2} on the RDE tip (Fig. 10a). All catalysts saw an increase in mass weighted exchange current density as a result of the NH_3 heat treatment. In particular, NH_3 treated NiMo/KB-NH_3 and NiMo/CNT-NH_3 showed the highest mass exchange current densities, with values of 3.6 ± 0.5 and 4.0 ± 0.4 A g^{-1}_{metal}, respectively. Comparable to Ni/N-CNTs (3.5 A g^{-1}_{metal}) and 20% Pd/C (5 ± 1 A g^{-1}_{metal}, for a particle diameter of 34 nm).[20,21] NiMo/CF(7%), demonstrated the next highest mass exchange current of 3.1 ± 0.5 A g^{-1}_{metal}, saw a threefold increase as a result of the NH_3 treatment. Moreover, the activities of NiMo/KB-NH_3, NiMo/CNT-NH_3 and NiMo/CF(7%)-NH_3 exceeded that of NiMo on 2D-MXene, reported at 2.09 A g^{-1}_{NiMo}.[6] In general, the mass exchange current densities reported in this study are likely underestimated due to the high catalyst loading of 500 • g cm^{-2}. The thick catalyst film is unlikely to see full utilization of its active material due to mass transport limitations, resulting in depressed mass weighted exchange current densities. To reinforce this hypothesis, the HOR currents did not increase proportionally with catalyst loading when going from 100 • g cm^{-2} to 500 • g cm^{-2} (Fig. S11). Still, the decision to use a loading of 500 • g cm^{-2} was to obtain larger nominal currents in the hope to bring out differences and similarities between the different synthesis methods.

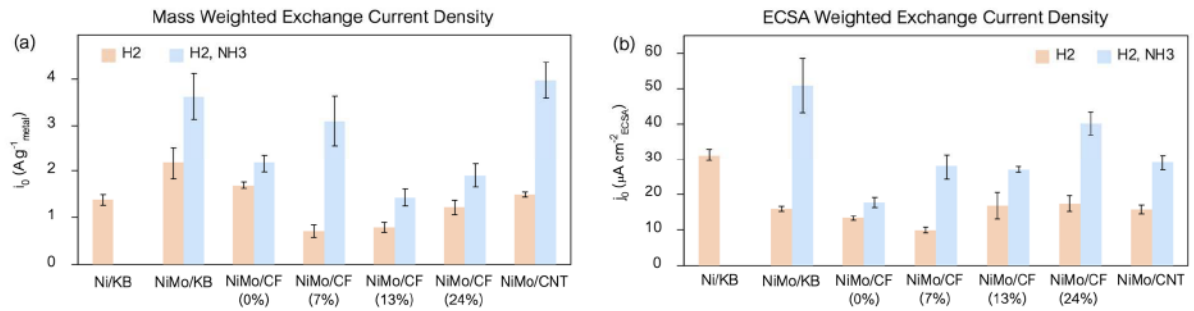

Figure 10. HOR performance metrics. (a) Mass weighted and (b) ECSA weighted exchange current densities obtained from LSVs measured between –0.06 V and 0.40 V in H_2 saturated 0.1M NaOH at a scan rate of 5 mV s^{-1} and 1600 rpm. The micro-polarization region, -10 mV < • < 10 mV, was linearized by least-squares fitting (Fig.

S4a). All R^2 values were at least 0.99. Error bars represent standard deviations of three independent experiments.

ECSA weighted exchange current densities were calculated to facilitate the comparison with state-of-the-art PGM-free HOR catalysts. As shown in Fig. 10b all catalysts saw an increase in specific activity as a result of the NH_3 heat treatment. The high specific exchange current density of molybdenum-free Ni/KB is not surprising given the inherent ability of Ni to catalyze hydrogen electrode reactions.[5] The role of the Mo is therefore not solely to improve the intrinsic activity of the Ni, but rather work as a passivation retardant. The delayed oxidation of NiMo was proposed by the XRD and XANES analysis (Fig. 4 and Fig. 5) and confirmed by CVs measured in N_2 saturated electrolyte (Fig. S9). The ECSA weighted exchange current densities for NiMo/KB-NH_3 and NiMo/CF(24%)-NH_3 were 50.9 ± 7.7 and 40.2 ± 3.2 • A cm^{-2}_{ECSA}, respectively, which outperform Ni/N-CNTs (28 • A cm^{-2}_{ECSA}) as well as untreated NiMo/KB, already an excellent non-PGM HOR catalyst first reported by Sadia et al. and here used as a benchmark.[17,20] Furthermore, NiMo/KB-NH_3 has an HOR activity comparable to Pd/C (60 ± 20 • A cm^{-2}_{ECSA}), 20% Pd/C Premtek (52 ± 2 • A cm^{-2}_{ECSA}), and Ru/C (64 • A cm^{-2}_{ECSA}).[21–23] In addition, NiMo/KB-NH_3 and NiMo/CF(24%)-NH_3 outperform CoNiMo, NiCu/C, Ni/Graphene and oxygen-vacancy-rich CeO_2-Ni (38 • A cm^{-2}_{ECSA}), while only NiMo/KB outperforms Ni/SC.[24–28] [3]

Kinetic current densities, extrapolated from Kouteki-Levich (KL) plots, are summarized in Fig. 11. Expressed as mass and ECSA weighted values, these current densities capture the HOR activity of the catalysts at 0.1 V, assuming no mass transport limitations. More specifically, this quantifier combines the intrinsic activity of the catalyst with its ability to withstand passivation and continue to perform the HOR at a slightly anodic potential. Of the catalysts only pyrolyzed in H_2, Ni/KB is no longer the best performing, according to this parameter (Fig. 11), despite having the largest specific exchange current density (Fig. 10b). This is because at a potential of 0.1 V its intrinsic catalytic capability is already having to compete with extensive passivation of Ni into α-$Ni(OH)_2$. This is supported by the weak dependency of current on rotation speed for Ni/KB (Fig. S10) quantified by an R^2 of 0.90 in the KL plot. The small R^2 indicates that

whatever is limiting the current at 0.1 V cannot be overcome by increasing the rotation speed. Hence, reactant availability and other mass transport effects are likely irrelevant. On the contrary, a reduction in the number of active sites due to passivation would explain the observed behavior. Similarly, NiMo/CF(7%), with an R^2 of 0.72, displays little to no dependence on transport phenomena at 0.1 V. However, the stagnant HOR currents are not due to Ni passivation, but rather a reduced intrinsic catalytic activity, demonstrated by the low exchange current density. NiMo/KB-NH_3 and NiMo/CF(24%)-NH_3 gave rise to the largest specific kinetic current densities, however, NiMo/CF(7%)-NH_3 and NiMo/CNT-NH_3 closely followed, in that order. The kinetic current densities calculated at 0.05 V and normalized by the geometric area of the electrode (ie. RDE glassy carbon tip, 0.247 cm^2) were 1.53 ± 0.21, 1.62 ± 0.17 and 2.01 ± 0.08 mA cm^{-2} for NiMo/KB-NH_3, NiMo/CF(7%)-NH_3 and NiMo/CNT-NH_3, respectively. These values outperformed the 1.12 mA cm^{-2} of NiMo on 2D-MXene and 1.73 mA cm^{-2} of oxygen-vacancy-rich CeO_2-Ni reported by Zhang et al. and Yang et al., respectively.[6,28]

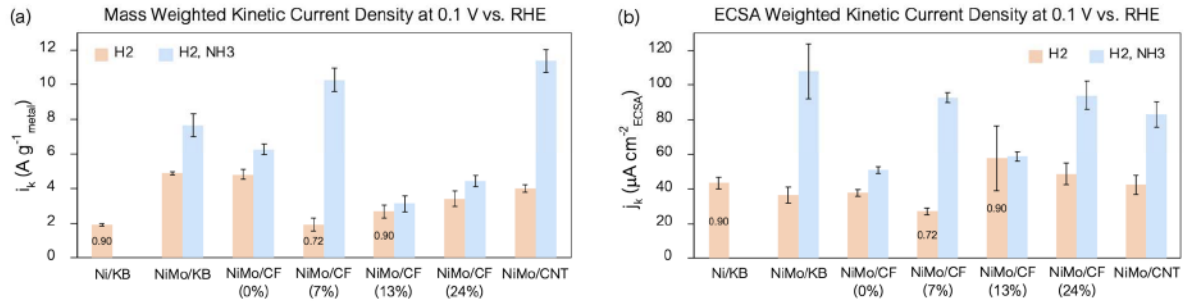

Figure 11. HOR performance metrics. (a) Mass weighted and (b) ECSA weighted kinetic current densities achieved at 0.1 V in H_2 saturated 0.1M NaOH at a scan rate of 5 mV s^{-1}. The catalyst loading was 500 • g cm^{-2}. These values were calculated from Koutecký-Levich plots (i^{-1} vs. • $^{-1/2}$), measured at various rotating speeds (400, 625, 900, 1600 and 2500 rpm), after linearization by least-squares fitting (Fig. S4b). All R^2 values were at least 0.98, when rounded to two significant figures, with the exception of three catalysts, whose R^2 values are reported in the plots. Error bars represent standard deviations of three independent experiments.

From the results in Fig. 8, 10 and 11, catalysts that underwent a heat treatment in NH_3 displayed higher HOR performance. Specifically, all catalysts showed higher kinetic and exchange current densities after the NH_3 treatment. However, improvement in the HOR

performance was uneven, with NiMo/KB, NiMo/CF(7%), NiMo/CF(24%) and NiMo/CNT benefiting the most from the NH_3 heat treatment. Furthermore, no one catalyst was the top performer for all three HOR performance quantifiers. NiMo/CF(7%)-NH_3 and NiMo/CNT-NH_3 jointly had the highest current densities at 0.1 V, while NiMo/KB-NH_3 and NiMo(24%CNT)-NH_3 showed the highest ECSA weighted kinetic current densities. These two catalysts also displayed the highest specific kinetic current density at 0.1 V, followed closely by NiMo/CF(7%)-NH_3 and NiMo/CNT-NH_3. The increase in the HOR performance after the NH_3 treatment is consistent with the works of Ni et. al and Song. et al., both ascribing the high HOR performance of their catalysts to the presence of Ni_3N.[2,8] Song et al. show through computation that interfacial Ni_3N/Ni sites supported on nickel foam (NF) have a hydrogen adsorption energy very close to zero: a property known to favor hydrogen electrochemistry.[2] Ni et al., also suggested weakening of the hydrogen bonding energy for their catalyst.[8] For the materials reported herein, structure-performance relations are not as lucid given that Ni_4N was detected in only half of the top performing HOR catalysts. The XRD and XANES characterization are both incapable of surface sensitivity, therefore the presence of interfacial nitrides on the other catalysts cannot be excluded. Furthermore, the presence of bulk Ni_4N does not rule out the existence of a more nitrogen-rich phase on the surface of the nanoparticles; in fact, it might even support it. The source of nitrogen was gas phase NH_3 reacting with the surface of the alloy nanoparticles. Hence, the presence of a thin Ni_3N layer—so thin to be undetectable by XRD and XANES—on the surface of the Ni_4N cannot be excluded.

In general, HOR activity slightly benefited from CNT-doping of the carbon fiber supports; nonetheless, this claim is to be made carefully. NiMo/CF(0%) did not excel in any of the HOR performance metrics. However, the same can be said for NiMo/CF(13%), disrupting the link between HOR performance and CNT-doping. Furthermore, NiMo/CF(13%) outperformed NiMo/CF(0%) only for ECSA weighted quantifiers, implying that the quality of alloy dispersion onto the carbon support factored into these trends. The high currents measured for NiMo/CF(7%)-NH_3 and NiMo/CF(24%)-NH_3, relative to NiMo/CF(0%)-NH_3, reinforce the conclusion that CNT-doping slightly enhanced the HOR performance. In particular, the specific exchange current density of

the NH_3 treated catalysts increased concurrently with the amount of CNT in the carbon fiber support (Fig. 10b). Zhuang et al. point to electronic effects between the nitrogen-doped CNT and the metal phase to explain the surprising HOR performance of Ni/N-CNT.[26] Specifically, they propose that the orbitals of Ni atoms located on the edge of nanoparticles were tuned by nitrogen atoms in the N-CNT support.[26] In our materials, the presence of nitrogen-doped CNT resulting from the NH_3 heat treatment cannot be excluded. However, the presence of such moieties and their consequent interaction with the active material were not investigated. Optimization of synthesis pathways, which is beyond the scope of this study, could lead to a more homogeneous dispersion of the metal nanoparticles on the carbon support and facilitate the investigation of NiMo-C, and potentially NiMo-N-C, interactions. An improved metal dispersion would also reduce discrepancies between the mass and ECSA weighted performance descriptors.

The HER activity of the four best HOR catalysts, as well as their NH_3 untreated precursors, was ascertained by rotating disk electrode. HER LSVs recorded in 0.1 M NaOH at a scan rate of 10 mV s^{-1} and 2500 rpm are shown in Fig. 12. The catalysts, with a loading of 50 • g_{metal} cm^{-2}, are benchmarked against commercial 10% Pt/C, 10 • g_{Pt} cm^{-2}. All catalysts reach 10 mA cm^{-2} with less than 350 mV overpotential, confirming the overall HER activity. Though Pt/C remains unmatched, NiMo/KB, NiMo/KB-NH_3 and NiMo/CNT-NH_3 show superior HER activity, comparable to that of functionalized Ni/C reported by Doan et al.[7] In fact, these three catalysts generate 25 mA cm^{-2} of current with less than 300 mV overpotential, despite their low catalyst loading. Based on Fig. 12, only NiMo/CF(7%) and NiMo/CNT show improved HER performance after the NH_3 heat treatment. This can be rationalized by the fact that current densities in Fig. 12 are normalized by geometric area as opposed to ECSA (Fig. 6). Catalysts with lower ECSA, such as NiMo/KB-NH_3 and NiMo/CF(24%)-NH_3, are somewhat penalized in Fig. 12. It follows that this plot is better used for benchmarking against Pt/C, rather than for a thorough comparison between NiMo catalysts. Fig. S12 shows the LSVs in Fig. 12 normalized by ECSA. This figure highlights the improved HER performance of NiMo/KB-NH_3 and NiMo/CF(24%)-NH_3 by correcting for losses in ECSA during the NH_3 treatment. Furthermore, these two materials saw the largest

increase in exchange current density (Fig. 10b): a descriptor of not only HOR but also HER performance.[29] Fig. S12 shows little improvement in specific HER activity for NiMo/CF(7%) and NiMo/CNT after the NH_3 treatment; this is especially true for NiMo/CNT. However, this is explained by the likely overestimated ECSAs for NiMo/CF(7%)-NH_3 and NiMo/CNT-NH_3 leading to depressed specific HER currents. Moreover, relative to NiMo/CF(7%), NiMo/CNT shows a smaller increase in the exchange current density after the NH_3 treatment.

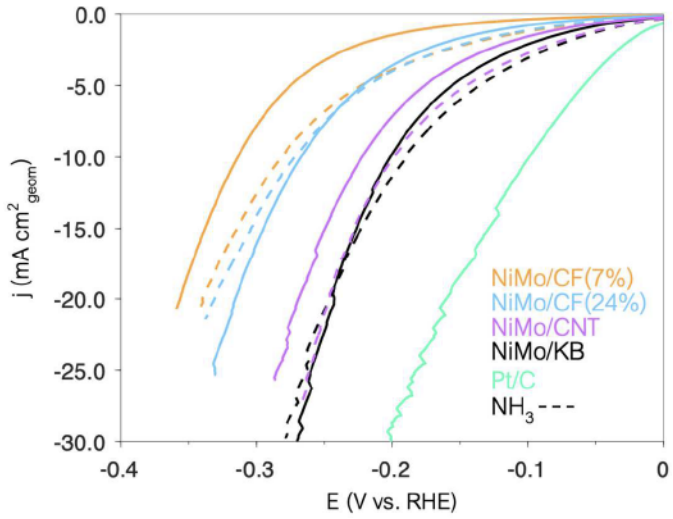

Figure 12. LSVs measured between 0.05 V and -0.6 V in N_2 saturated 0.1M NaOH at a scan rate of 10 mV s^{-1} and 2500 rpm. The loading was 50 • g_{metal} cm^{-2} for NiMo catalysts and 10 • g_{Pt} cm^{-2} for Pt/C. Dashed curves are for catalysts heat treated in NH_3. Curves are averages of three independent experiments.

Conclusion

Eleven PGM-free carbon supported NiMo catalysts were prepared, characterized and tested for HOR in alkaline media. The best performing catalysts were also active for HER. The NiMo alloyed nanoparticles were supported on CNT-doped carbon fibers, synthesized in-house by electrospinning, and benchmarked against Ni/KB and NiMo/KB. Successful integration of the CNTs with the electrospun fibers was verified by TEM, XRD and XANES. Together with STEM-EDS, these techniques confirmed a good dispersion of the metal nanoparticles on the carbon surface as well as the formation of a

NiMo alloy (9:1 atomic ratio). Additionally, XANES and XRD were used to monitor the effect of a second heat treatment in 10% NH_3 on the metallic phase of the catalysts. ECSAs were estimated by cyclic voltammetry taking into account the electrochemical contribution of the carbon support. HOR performance was evaluated using three quantifiers. First, the current density at 0.1 V, where NiMo/CF(7%)-NH_3 and NiMo/CNT-NH_3 gave the highest current of 1.51 ± 0.04 mA cm^{-2}, thereby surpassing many high performing catalysts, some containing PGMs. Mass and ECSA weighted exchange current densities were also calculated and compared to the state of the art. NiMo/KB-NH_3 and NiMo/CNT-NH_3, with mass exchange current densities of 3.6 ± 0.5 and 4.0 ± 0.4 A g^{-1}_{metal}, respectively, outperformed Ni/N-CNT (3.5 A g^{-1}_{metal}) and NiMo/2D-MXene (2.09 A g^{-1}_{NiMo}).[6,26] On an ECSA basis, NiMo/KB-NH_3 and NiMo/CF(24%)-NH_3 produced currents of 50.9 ± 7.7 and 40.2 ± 3.2 • A cm^{-2}_{ECSA}, respectively, surpassing oxygen-vacancy-rich CeO_2-Ni (38 • A cm^{-2}_{ECSA}), and approaching some PGM catalysts: Pd/C (60 ± 20 • A cm^{-2}_{ECSA}), 20% Pd/C Premtek (52 ± 2 • A cm^{-2}_{ECSA}) and Ru/C (64 • A cm^{-2}_{ECSA}).[15,21,28] Finally, kinetic current densities, obtained from KL plots, were used to capture HOR catalytic activity in the absence of mass transport limitations. At 0.05 V, NiMo/KB-NH_3 and NiMo/CF(24%)-NH_3 had the largest kinetic current densities, normalized by geometric area, and based on this indicator, outperformed oxygen-vacancy-rich CeO_2-Ni as well as NiMo/2D-MXene.[6,28] Heat treatment in NH_3 enhanced the HOR performance of all catalysts. In addition, HOR activity slightly benefited from CNT-doping of the carbon fiber support.

This study supports ongoing efforts to establish electrospinning as a technique for synthesizing carbon-based supports that are tunable (such as with CNT-doping) and robust, capable of withstanding subsequent heat treatments, usually required in the preparation/annealing of metallic nanoparticles. Furthermore, electrochemical data emphasized that NH_3 treating carbon supported nickel-based catalysts results in substantial (up to five-fold) increases in the HOR performance. Finally, based on the electrochemical results, we conclude that the NH_3 heat treatment also improved HER activity, thus promoting nickel's ability to catalyze both the HER and HOR in alkaline media.

Corresponding Author

Plamen Atanassov • Department of Chemical and Biomolecular Engineering, University of California, Irvine, California 92697, USA

Conflicts of Interest

There are no conflicts to declare.

Acknowledgements

The authors acknowledge the use of facilities and instrumentation at the UC Irvine Materials Research Institute (IMRI), which is supported in part by the National Science Foundation through the UC Irvine Materials Research Science and Engineering Center (DMR-2011967). This work has been supported in part by the National Science Foundation (NSF) through the International Research Experiences for Students (IRES) program (NSF-2107534).

References

[1] S. Kabir, K. Lemire, K. Artyushkova, A. Roy, M. Odgaard, D. Schlueter, A. Oshchepkov, A. Bonnefont, E. Savinova, D.C. Sabarirajan, P. Mandal, E.J. Crumlin, I. V. Zenyuk, P. Atanassov, A. Serov, Platinum group metal-free NiMo hydrogen oxidation catalysts: High performance and durability in alkaline exchange membrane fuel cells, J Mater Chem A Mater. 5 (2017) 24433–24443. https://doi.org/10.1039/C7TA08718G.

[2] F. Song, W. Li, J. Yang, G. Han, P. Liao, Y. Sun, Interfacing nickel nitride and nickel boosts both electrocatalytic hydrogen evolution and oxidation reactions, Nat Commun. 9 (2018). https://doi.org/10.1038/s41467-018-06728-7.

[3] Y. Duan, Z.Y. Yu, L. Yang, L.R. Zheng, C.T. Zhang, X.T. Yang, F.Y. Gao, X.L. Zhang, X. Yu, R. Liu, H.H. Ding, C. Gu, X.S. Zheng, L. Shi, J. Jiang, J.F. Zhu,

M.R. Gao, S.H. Yu, Bimetallic nickel-molybdenum/tungsten nanoalloys for high-efficiency hydrogen oxidation catalysis in alkaline electrolytes, Nat Commun. 11 (2020). https://doi.org/10.1038/S41467-020-18585-4.

[4] Y. Xue, L. Shi, X. Liu, J. Fang, X. Wang, B.P. Setzler, W. Zhu, Y. Yan, Z. Zhuang, A highly-active, stable and low-cost platinum-free anode catalyst based on RuNi for hydroxide exchange membrane fuel cells, Nat Commun. 11 (2020). https://doi.org/10.1038/s41467-020-19413-5.

[5] E.S. Davydova, S. Mukerjee, F. Jaouen, D.R. Dekel, Electrocatalysts for Hydrogen Oxidation Reaction in Alkaline Electrolytes, ACS Catal. 8 (2018) 6665–6690. https://doi.org/10.1021/ACSCATAL.8B00689.

[6] T. Zhang, S. Debow, F. Song, Y. Qian, W.R. Creasy, B.G. Delacy, Y. Rao, Interface Catalysis of Nickel Molybdenum (NiMo) Alloys on Two-Dimensional (2D) MXene for Enhanced Hydrogen Electrochemistry, J. Phys. Chem. Lett. 2021. 12 (2021). https://doi.org/10.1021/acs.jpclett.1c02676.

[7] H. Doan, I. Kendrick, R. Blanchard, Q. Jia, E. Knecht, A. Freeman, T. Jankins, M.K. Bates, S. Mukerjee, Functionalized Embedded Monometallic Nickel Catalysts for Enhanced Hydrogen Evolution: Performance and Stability, J Electrochem Soc. 168 (2021) 084501. https://doi.org/10.1149/1945-7111/ac11a1.

[8] W. Ni, A. Krammer, C. Hsu, H.M. Chen, A. Schüler, X. Hu, Ni 3 N as an Active Hydrogen Oxidation Reaction Catalyst in Alkaline Medium , Angewandte Chemie. 131 (2019) 7523–7527. https://doi.org/10.1002/ange.201902751.

[9] F.Y. Gao, S.N. Liu, J.C. Ge, X.L. Zhang, L. Zhu, Y.R. Zheng, Y. Duan, S. Qin, W. Dong, X. Yu, R.C. Bao, P.P. Yang, Z.Z. Niu, Z.G. Ding, W. Liu, S. Lan, M.R. Gao, Y. Yan, S.H. Yu, Nickel–molybdenum–niobium metallic glass for efficient hydrogen oxidation in hydroxide exchange membrane fuel cells, Nature Catalysis 2022 5:11. 5 (2022) 993–1005. https://doi.org/10.1038/s41929-022-00862-8.

[10] E.S. Davydova, S. Mukerjee, F. Jaouen, D.R. Dekel, Electrocatalysts for Hydrogen Oxidation Reaction in Alkaline Electrolytes, ACS Catal. 8 (2018) 6665–6690. https://doi.org/10.1021/acscatal.8b00689.

[11] X. Mu, S. Liu, L. Chen, S. Mu, Alkaline Hydrogen Oxidation Reaction Catalysts: Insight into Catalytic Mechanisms, Classification, Activity Regulation and Challenges, (2022). https://doi.org/10.1002/sstr.202200281.

[12] T. Asset, A. Roy, T. Sakamoto, M. Padilla, I. Matanovic, K. Artyushkova, A. Serov, F. Maillard, M. Chatenet, K. Asazawa, H. Tanaka, P. Atanassov, Highly active and selective nickel molybdenum catalysts for direct hydrazine fuel cell, (2016). https://doi.org/10.1016/j.electacta.2016.08.106.

[13] D. Wang, Q. Li, C. Han, Z. Xing, X. Yang, When NiO@Ni Meets WS2 nanosheet array: A highly efficient and ultrastable electrocatalyst for overall water splitting, ACS Cent Sci. 4 (2018) 112–119. https://doi.org/10.1021/ACSCENTSCI.7B00502/SUPPL_FILE/OC7B00502_SI_001.PDF.

[14] W. Sheng, H.A. Gasteiger, Y. Shao-Horn, Hydrogen Oxidation and Evolution Reaction Kinetics on Platinum: Acid vs Alkaline Electrolytes, J Electrochem Soc. 157 (2010) B1529. https://doi.org/10.1149/1.3483106.

[15] J. Durst, A. Siebel, C. Simon, F. Hasché, J. Herranz, H.A. Gasteiger, New insights into the electrochemical hydrogen oxidation and evolution reaction mechanism, Energy Environ Sci. 7 (2014) 2255–2260. https://doi.org/10.1039/C4EE00440J.

[16] Z. Li, L. An, M. Song, T. Zhao, J. Zhang, C. Zhang, Z. Li, D. Wang, Tuning the hydrogen and hydroxyl adsorption on Ru nanoparticles for hydrogen electrode reactions via size controlling, Chinese Chemical Letters. 34 (2023). https://doi.org/10.1016/j.cclet.2022.06.045.

[17] S. Kabir, K. Lemire, K. Artyushkova, A. Roy, M. Odgaard, D. Schlueter, A. Oshchepkov, A. Bonnefont, E. Savinova, D.C. Sabarirajan, P. Mandal, E.J. Crumlin, I. V. Zenyuk, P. Atanassov, A. Serov, Platinum group metal-free NiMo

hydrogen oxidation catalysts: High performance and durability in alkaline exchange membrane fuel cells, J Mater Chem A Mater. 5 (2017) 24433–24443. https://doi.org/10.1039/c7ta08718g.

[18] D.S. Hall, C. Bock, B.R. MacDougall, The Electrochemistry of Metallic Nickel: Oxides, Hydroxides, Hydrides and Alkaline Hydrogen Evolution, J Electrochem Soc. 160 (2013) F235–F243. https://doi.org/10.1149/2.026303JES/XML.

[19] J. Durst, A. Siebel, C. Simon, F. Hasché, J. Herranz, H.A. Gasteiger, New insights into the electrochemical hydrogen oxidation and evolution reaction mechanism, Energy Environ Sci. 7 (2014) 2255–2260. https://doi.org/10.1039/c4ee00440j.

[20] Z. Zhuang, S.A. Giles, J. Zheng, G.R. Jenness, S. Caratzoulas, D.G. Vlachos, Y. Yan, Nickel supported on nitrogen-doped carbon nanotubes as hydrogen oxidation reaction catalyst in alkaline electrolyte, Nature Communications 2016 7:1. 7 (2016) 1–8. https://doi.org/10.1038/ncomms10141.

[21] J. Zheng, S. Zhou, S. Gu, B. Xu, Y. Yan, Size-Dependent Hydrogen Oxidation and Evolution Activities on Supported Palladium Nanoparticles in Acid and Base, J Electrochem Soc. 163 (2016) F499–F506. https://doi.org/10.1149/2.0661606JES/XML.

[22] J. Durst, A. Siebel, C. Simon, F. Hasché, J. Herranz, H.A. Gasteiger, New insights into the electrochemical hydrogen oxidation and evolution reaction mechanism, Energy Environ Sci. 7 (2014) 2255–2260. https://doi.org/10.1039/C4EE00440J.

[23] J. Ohyama, T. Sato, Y. Yamamoto, S. Arai, A. Satsuma, Size specifically high activity of ru nanoparticles for hydrogen oxidation reaction in alkaline electrolyte, J Am Chem Soc. 135 (2013) 8016–8021. https://doi.org/10.1021/JA4021638/SUPPL_FILE/JA4021638_SI_001.PDF.

[24] W. Sheng, A.P. Bivens, M. Myint, Z. Zhuang, R. V. Forest, Q. Fang, J.G. Chen, Y. Yan, Non-precious metal electrocatalysts with high activity for hydrogen oxidation reaction in alkaline electrolytes, Energy Environ Sci. 7 (2014) 1719–1724. https://doi.org/10.1039/C3EE43899F.

[25] O. V. Cherstiouk, P.A. Simonov, A.G. Oshchepkov, V.I. Zaikovskii, T.Y. Kardash, A. Bonnefont, V.N. Parmon, E.R. Savinova, Electrocatalysis of the hydrogen oxidation reaction on carbon-supported bimetallic NiCu particles prepared by an improved wet chemical synthesis, Journal of Electroanalytical Chemistry. 783 (2016) 146–151. https://doi.org/10.1016/J.JELECHEM.2016.11.031.

[26] Z. Zhuang, S.A. Giles, J. Zheng, G.R. Jenness, S. Caratzoulas, D.G. Vlachos, Y. Yan, Nickel supported on nitrogen-doped carbon nanotubes as hydrogen oxidation reaction catalyst in alkaline electrolyte, Nat Commun. 7 (2016). https://doi.org/10.1038/NCOMMS10141.

[27] F. Yang, X. Bao, Y. Zhao, X. Wang, G. Cheng, W. Luo, Enhanced HOR catalytic activity of PGM-free catalysts in alkaline media: the electronic effect induced by different heteroatom doped carbon supports, J Mater Chem A Mater. 7 (2019) 10936–10941. https://doi.org/10.1039/C9TA01916B.

[28] F. Yang, X. Bao, P. Li, X. Wang, G. Cheng, S. Chen, W. Luo, Boosting Hydrogen Oxidation Activity of Ni in Alkaline Media through Oxygen-Vacancy-Rich CeO2/Ni Heterostructures, Angewandte Chemie International Edition. 58 (2019) 14179–14183. https://doi.org/10.1002/ANIE.201908194.

[29] J. Durst, C. Simon, F. Hasché, H.A. Gasteiger, Hydrogen Oxidation and Evolution Reaction Kinetics on Carbon Supported Pt, Ir, Rh, and Pd Electrocatalysts in Acidic Media, J Electrochem Soc. 162 (2015) F190–F203. https://doi.org/10.1149/2.0981501JES.